

Investigation on the Corrosion Resistance of T4C Titanium Alloy in Simulated Oilfield Solution

Xiang-hong LÜ¹, Xin-xin ZHANG^{1*}, Hong-fu LI², Long CHEN³, Chen WANG¹, Jian LI, Yan-ming LIU¹, Ning Li¹, Jing-yu DENG¹, Wen-long ZHENG¹

¹ School of Materials Science and Engineering, Xi'an Shiyou University, Xi'an 710065, People's Republic of China

² Oil-Gas Storage and Transportation Company, PetroChina Xinjiang Oilfield, Karamay 831100, People's Republic of China

³ Research Institute of Engineering Technology, PetroChina Xinjiang Oilfield Company, Karamay 831100, People's Republic of China

*E-mail: 1589847792@qq.com

Received: 7 September 2022 / Accepted: 29 October 2022 / Published: 17 November 2022

Based on the corrosion rates under high-temperature and high-pressure, both the corrosion behaviors of TC4 titanium alloy tubes in neutral and acidic (containing CO₂ and H₂S) environments and the thermodynamic stability of their passivation films were investigated by in-situ electrochemical tests combined with molecular dynamics simulations and first-principles calculations. The results show that the corrosion of TC4 titanium alloy at 180 °C is mild. And the corrosion reaction of TC4 titanium alloy in different environments is controlled by an anodic reaction process. Comparing with the neutral environment, TC4 titanium alloy in CO₂ and H₂S environment present smaller electrochemical corrosion kinetic resistance. Among three environments, TC4 titanium alloy shows the worst corrosion resistance in H₂S environment. Cl⁻, HCO₃³⁻ and HS⁻, all have strong charge interactions with the positive-charged Ti atoms of TiO₂(110) passivation surface. By altering Cl⁻ concentration and temperature, the existence of H₂S and CO₂ will reduce the binding energy between Cl⁻ and TiO₂(110) surface, i.e., the thermodynamic stability of the TiO₂ passivation film became worse.

Keywords: TC4 titanium alloy; corrosion resistance mechanism; thermodynamic stability; molecular dynamics (MD) simulation; first-principles calculation

1. INTRODUCTION

With the worldwide increasing demand for oil and gas resources, the exploitation of oil and gas fields has gradually drilled much deeper. According to a survey, over 11 % offshore wells will have higher than 175 °C bottom-hole temperatures in the next three or five years. Moreover, the bottom hole

pressure is between 70~100MPa for nearly 26 % wells while the predicted bottom hole pressure is higher than 100MPa and contains CO₂, H₂S and Cl⁻[1] for 5 % wells. Thus, oil pipes with both high-strength and corrosion-resistant are urgently needed under the aforementioned harsh conditions. Titanium alloy pipe has attracted extensive attention because of its excellent corrosion resistance and mechanical properties[2,3]. Since the mid-1980s, titanium alloy has been utilized in the manufacturing of casing, tubing and some downhole tools, which aims at oil and gas wells under high-pressure and high-temperature, even ultra-high-pressure and ultra-high-temperature (such as the Gulf of Mexico)[4,5]. Unocal employed Ti-3Al-8V-6Cr-4Mo-4Zr alloy pipe for the hot brine geothermal well (temperature over 300 °C) in the Salton Sea region of the United States; RMI Titanium Corporation harnessed Ti-6Al-4V-Ru tubing in Mobile Bay Field hot-acid oil and gas well (high concentrations of NaCl, H₂S and CO₂ at bottom hole temperature up to 235 °C); Chevron is also actively developing Ti-6Al-2Sn-4Zr-6Mo, Ti-6Al-4V and Ti-6Al-4V-Ru[6~8] alloy used for oil and gas well.

In fact, titanium is an active metal, and its corrosion resistance mainly stems from the passivation film (stable, dense titanium oxide layer) on its surface[9~11]. Titanium and oxygen can form various compounds with different Ti/O ratios and different structures, such as TiO₂, TiO, Ti₃O₄, Ti₂O₃, etc. In general, a 5~10 nm thick TiO₂ oxide film (passivating film)[12,13] can be rapidly formed on the surface of fresh titanium, which may exist in three polymorphs: rutile, anatase, and brookite[14~16]. All these phases are composed of octahedral structures, but their arrangement, bonding and lattice structures are different[16]. The TiO₂ rutile phase belongs to the tetragonal crystal structure, and its molecular formula is Ti₂O₄ per unit cell. The TiO₂ anatase phase has same crystal structure, while its molecular formula is Ti₄O₈ per unit cell. The TiO₂ brookite phase belongs to the rhombic crystal structure and its molecular formula is Ti₆O₁₂ per unit cell. The rutile phase is thermodynamic stable under ambient conditions, and is identified as the main component of titanium alloy's passivation film. Therefore, the excellent corrosion resistance of titanium alloy pipe can be ascribed to the thermodynamic stability of its passivation film[17,18]. However, the studies about titanium alloy's passivation film, such as its formation process, film composition, structure, performance and thermodynamic stability, are still insufficient up to now.

Therefore, based on the experimental data, we discussed the thermodynamic stability and corrosion resistance mechanism of titanium alloy's passivation film in this paper by implementing in situ electrochemical analysis and MD simulations.

2. EXPERIMENTAL

2.1 Corrosion tests

2.1.1 Materials and test specimen

All the specimen were cut from TC4 (110ksi (758MPa) grade) titanium alloy tubing with size of $\Phi 88.9\text{mm} \times 6.45\text{mm}$, chemical composition of which is (wt.%): Al: 6.0;V: 4.2 ;Fe : 0.04 ;C: 0.01 ; N: 0.01 ; O, 0.09 ; Ti :Balance. The high-temperature and high-pressure weight loss test sample size was

50mm×10mm×3mm. These samples were polished with abrasive paper up to 1,200#, leading to surface roughness $\leq 1.6\mu\text{m}$; the electrochemical test sample was a circular sheet sample with working area of 1 cm^2 and 3 mm thickness.

2.1.2 Methodology and details

(1) High-temperature and high-pressure weight loss test

The aqueous medium, which is simulated oilfield solution composed of deionized water and main ions shown in table 1. were neutral (no CO_2 or H_2S) and acidic (including CO_2 or H_2S) respectively. The neutral corrosive environment is achieved by charging N_2 2 hours in the solution. Partial pressure of CO_2 , as well as H_2S , was 2 MPa (total pressure is 10 MPa). The immersion tests were carried out under 180 °C set temperature in the simulated oilfield solution for 360 h using TFCZ5-35/250 magnetic reaction auto-clave.

Table 1. Corrosion test conditions

Corrosion environment	Neutral	CO_2	H_2S
Temperature/°C		180	
CO_2 partial pressure/MPa	0	0	2
H_2S partial pressure//MPa	0	2	0
Total pressure/MPa	10 (inlet N_2)		
Aqueous medium/ $\text{mg}\cdot\text{L}^{-1}$	NaHCO_3 : 850; Na_2SO_4 : 170; CaCl_2 : 11000; MgCl_2 : 2943; NaCl :247371; KCl :3821		

(2) Electrochemical test

the electrochemical test chose AMETEK 273A potentiostat and M5210 lock-in amplifier. A large area of Pt sheet was used as the counter electrode (CE), and an Ag/AgCl electrode was used as the reference electrode (RE). The solution was same as the corrosion test. The potentiodynamic polarization curves were measured starting at -500mV with a scanning rate of 0.3333 mV/s. Cyclic potentiodynamic polarization was performed from a negative potential at -500 mV up to sweepback potential at +1600mV or the flyback current was 1mA with a sweep rate of 20 mV/s. Electrochemical Impedance Spectroscopy (EIS) tests were conducted from 100 kHz to 5mHz with 10 mV peak-to-peak linear sinusoidal perturbation. And 1000 Hz Mott–Schottky frequency, -1.0~-0.2 V scanning interval, 5 mV AC voltage amplitude and 5mV step potential was adopted. In addition, it should be noted that all potentials in this paper were referred to Ag/AgCl (vs OPE).

2.2 Modeling and simulations

2.2.1 First-principles calculations

The rutile phase (TiO_2) crystal belongs to a tetragonal structure with space group $P42/MNM$ [19]. First, the surface supercell of $\text{TiO}_2(110)$ (2×1) was constructed. Second, the vacuum layer is inserted to avoid the imaginary interaction between top and bottom sides. Third, the interface models are established by putting adsorbate (molecules and ions) over the surfaces. The interface models are shown as Fig. 1.

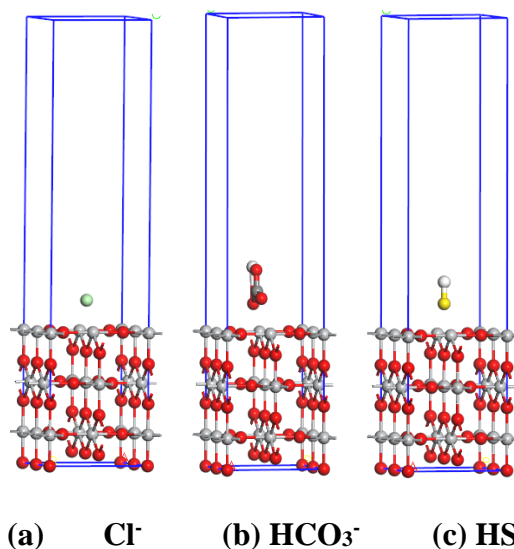


Figure 1. Interface models of corrosive ions' adsorption onto rutile $\text{TiO}_2(110)$

The plane-wave ultrasoft pseudo-potential formalism based on the density functional theory (DFT) was used for all calculations. Under the framework of generalized gradient approximation (GGA), the exchange and correlation potentials were determined by the PBE functional form, and the Kohn-Sham equation was self-consistently solved. The ultrasoft pseudopotential was adopted to describe the interaction between valence electrons and ions. The maximum cutoff energy calculated by a plane wave in reciprocal space was $E_{\text{cut}} = 420$ eV. Self-consistent calculation convergence accuracy reached 5×10^{-7} eV/atom.

2.2.2 Molecular dynamics (MD) simulations

The $\text{TiO}_2(110)$ (10×5) surface models were constructed, then the vacuum layer was inserted, and the adsorbate (molecules and ions) were put over the surfaces to establish interface models.

On the basis of actual operating conditions of oilfield, the Cl^- concentration of $50000 \text{ mg} \cdot \text{L}^{-1}$ and $100000 \text{ mg} \cdot \text{L}^{-1}$ were considered respectively. In the aqueous medium, 30 and 60 Cl^- ions were contained for the both concentrations. All the partial pressures of CO_2 and H_2S were 5MPa. For the numbers of HCO_3^- and HS^- ions, which are mainly formed by ionization of CO_2 and H_2S in aqueous solution, the

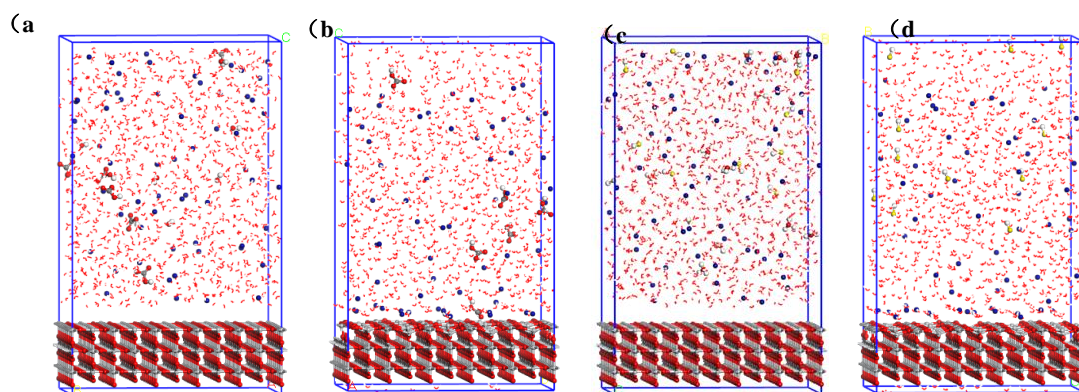
gas solubility model established by Duan et al.[20] was adopted in the present work. Various temperatures of 120, 180 and 230 °C were also considered.

Fig. 2 shows the optimized interface models. It can be seen that a very thin disordered atoms layer were formed onto the surface after optimization due to a reaction between surface and aqueous solution.

Based on the configurations of optimized interface models, the interfacial binding energy was calculated according to the following equation:

$$E_{\text{interface}} = (E_{\text{total}} - E_{\text{ion}} - E_{\text{TiO}_2}) / S \quad (1)$$

Where S is the interface area, E_{total} is the total energy after optimization of the whole system. E_{ion} and E_{TiO_2} are the energy of the aqueous solution and TiO₂ surface, respectively.



(a)CO₂ environment (before optimization) (b) CO₂ environment (after optimization) (c) H₂S environment (before optimization) (d) H₂S environment (after optimization)

Figure 2. Interface model of TiO₂ (110) crystal surface before and after geometric optimization (partial pressure of CO₂ and H₂S: 10MPa;Cl⁻: 100000 mg/L;Temperature: 230 °C)

In the molecular dynamics simulations, periodic boundary conditions were adopted, which can avoid the boundary effect caused by the size limit of the established model[21].The molecular dynamics simulation was performed using COMPASS forcefield, and the Ewald summation and the van der Waals electrostatic interaction were utilized.

3. RESULTS AND DISCUSSION

3.1 Pitting and uniform corrosion

Fig.3 and Fig.4 present the surface and cross-section micro corrosion morphology of TC4 titanium alloy samples after the high-temperature and high-pressure corrosion test. It is cleared that uniform corrosion on the surface of all samples was slight in three environments, with no obvious pitting. Fig.5 shows the comparative analysis of the uniform corrosion rate of TC4 titanium alloy in CO₂ and H₂S environments. Corrosion rate of titanium alloy is only 0.0004 mm·a⁻¹, 0.0004 mm·a⁻¹ and 0.0009mm·a⁻¹ respectively around the high-temperature environment of 180 °C. Although the corrosion-

resistant properties of TC4 titanium alloy are relatively weak in an H₂S environment, the uniform corrosion degree was extremely mild according to the standard NACE SP 0755-2013[22]. It is can still believed that titanium alloys have good corrosion resistance in harsh underground working conditions.

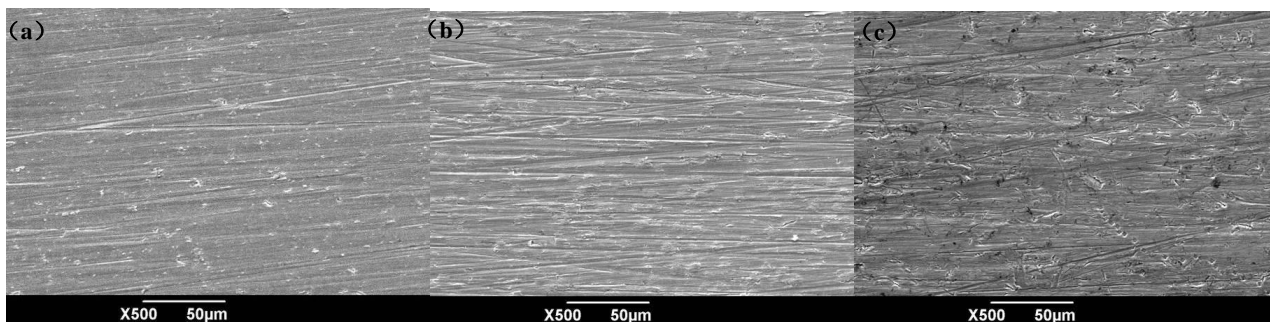


Figure 3. Surface corrosion morphologies of TC4 alloys in neutral(a) CO₂(b) and H₂S (c) environments(180°C)

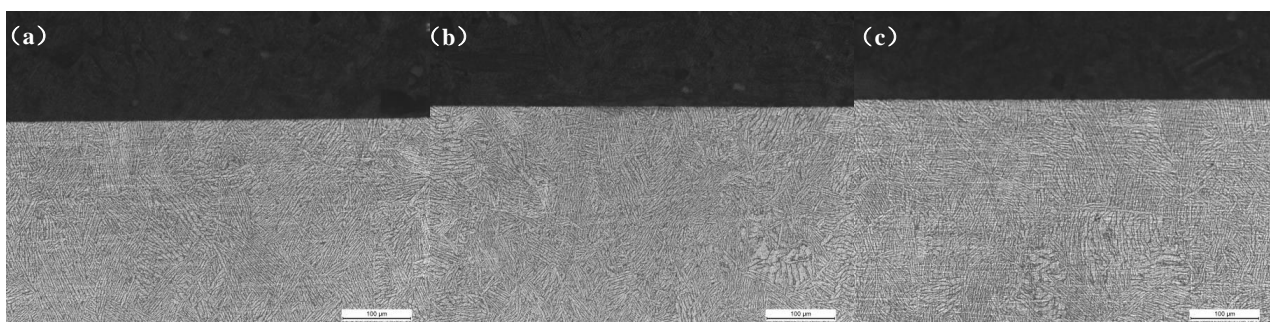


Figure 4. Cross-section corrosion morphologies of TC4 alloys in neutral(a), CO₂(b) and H₂S (c) environments(180°C)

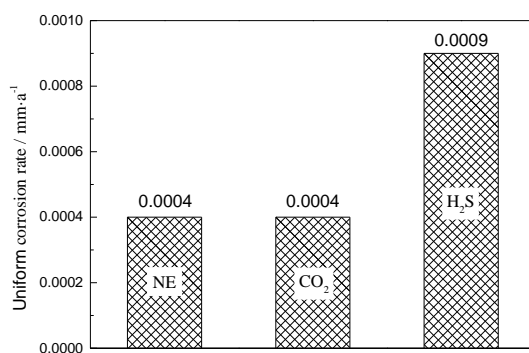


Figure 5. The uniform corrosion rate of TC4 alloys in different environments(180°C)

3.2 Electrochemical properties of passivation films

3.2.1 Polarization curves and cyclic polarization curves

Figure 6 shows the results of the polarization curves and cyclic polarization curves of TC4 titanium alloy in neutral, CO₂ and H₂S environments. In the three corrosion environments, the anodic polarization curves of titanium alloys all showed obvious passivation areas, which indicate the corrosion reaction was controlled by the anodic reaction process. At the same time, the reverse scan polarization curve and forward scan polarization curve all intersect at the anode polarization region, it means that TC4 titanium alloy has a high level of passivation and re-passivation in the simulated downhole corrosion environment. Table 2 shows the fitting and analysis results of corrosion potential, corrosion current density, breakdown potential (E_b) and protection potential (E_{pr}) of titanium alloys in different corrosion environments. E_b of TC4 titanium alloy in CO₂ and H₂S environments decreased gradually compared with a neutral environment. Moreover, E_{pr} of TC4 titanium alloy is not much different in neutral and CO₂ environments while that is significantly reduced in the H₂S environment. As the protective potential (E_{pr}) is the most important index to characterize the stability of the passivating film, the stability of TC4 passivation film in the H₂S environment is relatively poor, the corrosion current density is relatively high, and the corrosion resistance is reduced[23].

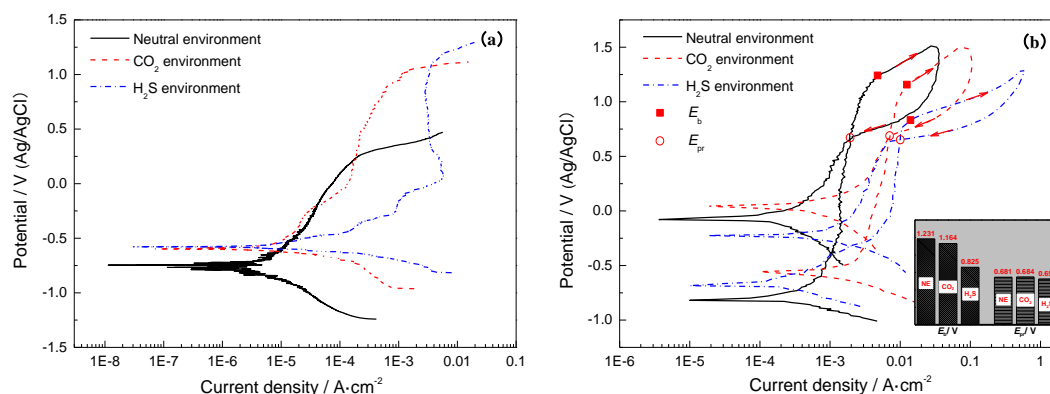


Figure 6. Polarization curves(a) and cyclic polarization curves(b) of TC4 alloys in different environments(180°C)

Table 2. Electrochemical parameters of TC4 alloys in different environments (180°C)

Corrosion environment	Corrosion potential E_c /V	Corrosion current density I_c /A·cm ⁻²	Breakdown potential E_b /V	Repassivation potential E_{pr} /V
Neutral	-0.745	4.1756×10 ⁻⁶	1.231	0.681
CO ₂	-0.600	1.1909×10 ⁻⁵	1.164	0.684
H ₂ S	-0.577	1.7588×10 ⁻⁵	0.825	0.655

3.2.2 EIS

Fig.7 shows the EIS plots and their equivalent circuits of TC4 titanium alloy in neutral, CO₂ and H₂S environments. The EIS plots of TC4 titanium alloy have three-time constants in the three corrosion environments, among which the capacitive resistance in the high-frequency zone is associated with the resistance capacitive relaxation process composed of reaction transfer resistance and electrode interface capacitance. The capacitive reactance arc in the low-frequency region is the superposition of two capacitive reactance arcs, and the corresponding state variables are the particle adsorption rate at the electrode/solution interface and the potential difference of the passivating film, in which the passivating film can be regarded as an independent variable in series with other variables.

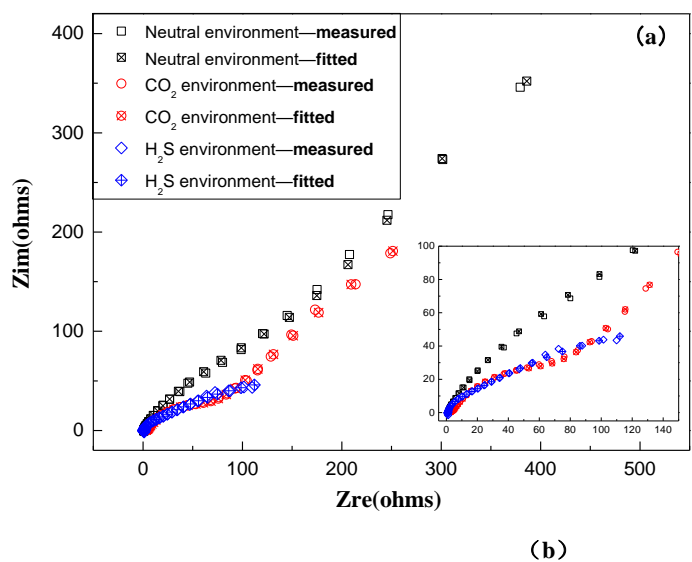


Figure 7. EIS plots (a) and equivalent circuit (b) of TC4 alloys in different environments (180°C)

Table 3 shows the fitting results of TC4 titanium alloy EIS plot in different corrosion environments, where R_s is the solution resistance, R_t is the charge transfer resistance, C_{dl} is the double-layer capacitance of passivation film/solution interface, C_c and R_c are the double-layer capacitance and resistance of adsorption particles on the electrode surface, C_m and R_m are the double-layer capacitance and resistance of passivation film. It can be seen in Table 3 that both membrane resistance R_m decreases and the protective effect of passivation film decrease successively (in the H₂S environment, R_m decreases

significantly) in the neutral, CO₂ and H₂S environments. Taking the real part of $\omega \rightarrow 0$ minus the real part of $\omega \rightarrow \infty$ on the EIS plots to calculate the polarization resistance of TC4 titanium alloy in neutral, CO₂ and H₂S environments, which are respectively 2691.18 $\Omega \cdot \text{cm}^2$, 1632.10 $\Omega \cdot \text{cm}^2$, 308.22 $\Omega \cdot \text{cm}^2$. The electrochemical corrosion resistance is gradually reduced[24]. Obviously, the corrosion resistance of TC4 titanium alloy at high temperatures with H₂S is relatively poor[25,26].

Table 3. Fitted results for EIS measured in different environments (180°C)

Corrosion environment	R_s $\Omega \cdot \text{cm}^2$	C_{dl} $\text{F} \cdot \text{cm}^{-2}$	R_t $\Omega \cdot \text{cm}^2$	C_c $\text{F} \cdot \text{cm}^{-2}$	R_c $\Omega \cdot \text{cm}^2$	C_m $\text{F} \cdot \text{cm}^{-2}$	R_m $\Omega \cdot \text{cm}^2$
Neutral	1.073	0.001742	517	2.656E-5	0.1027	0.00514	2172
CO ₂	2.708	4.837E-6	66.79	0.001132	1.598	0.0116	2061
H ₂ S	1.177	0.002999	272.4	0.02583	11.93	0.003547	22.71

3.2.3 Mott-Schottky (M-S) curves

Generally, the passivating film on a metal surface is semiconductor, which is divided into n-type semiconductors and p-type semiconductors. A p-type semiconductor is characterized by anion selectivity and an n-type semiconductor is characterized by cation selectivity. This characteristic of the passivating film can effectively prevent erosion in solution[27]. Fig. 8 shows the M-S curve of TC4 titanium alloy in neutral, CO₂ and H₂S environments. The M-S curve of titanium alloy under three corrosion conditions only has a positive slope range, indicating the passivation film of titanium alloy is an n-type semiconductor. Therefore, it has cation selectivity and can repel the erosion of metal matrix by Cl⁻, thus endowing TC4 titanium alloy with strong corrosion resistance. According to the Mott-Schottky relation (where in the dielectric constant ϵ of the semiconductor is taken as 114)[28~31], the donor concentration and the flat band potential in the titanium alloy passivation film are shown in Table 4. Relevant data show[32,33]that the higher the concentration of donor and acceptor in the passivating film, the faster the diffusion rate of ions, the worse the stability of the passivating film, and the higher the corrosion rate. Table 4 shows that the donor concentration of TC4 titanium alloy passivation membrane in neutral, CO₂ and H₂S environment gradually increased under 180 °C high temperature condition. Therefore, compared with the neutral and CO₂ environments, the corrosion resistance of TC4 titanium alloy decreases in the H₂S environment, which is also consistent with the above test and analysis results.

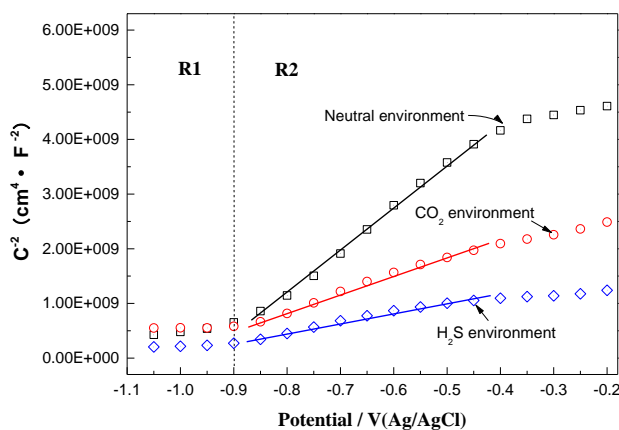


Figure 8. M-S curve of TC4 alloys in different environments (90°C)

Table 4. The doping concentration and flat band potential of TC4 alloys passivation film in different environments (90°C)

Corrosion environment	N_D (cm^{-3})	E_{fb} (V)
Neutral	1.983×10^{18}	-0.953
CO ₂	4.125×10^{18}	-1.021
H ₂ S	7.367×10^{18}	-1.052

3.3 Passivation film thermodynamic stability

3.3.1 Electronic structure of the interface between different aggressive ions and TiO₂(110)

Figure 9(a)~(c) shows the charge density distribution of a single Cl⁻ ion, a single HCO³⁻ ion, and a single HS⁻ ion adsorbed on the surface of TiO₂(110), respectively. In Fig.9, electrons are biased between the O atoms in Cl⁻ ions, HCO³⁻ ions, S atoms of HS⁻ ions and Ti atoms on the TiO₂ surface when the adsorption reaches the steady-state. It indicated that there is a strong charge interaction with the positively charged Ti atoms on the TiO₂(110) surface for the three negatively charged aggressive ions of Cl⁻, HCO³⁻ and HS⁻[34]. To verify the above conclusion, the steady-state adsorption configurations of Cl⁻, HCO³⁻, and HS⁻ on the TiO₂(110) surface were analyzed by differential charge density analysis, as shown in Figure 10. As seen from the plots, there is charge bias around the O atom in Cl⁻ ion, HCO³⁻ ion, and S atom in HS⁻ ion as the adsorption reaches the steady-state, while there is charge dissipation near the Ti atom on the TiO₂ surface. Therefore, the interfacial bonding is mainly due to the charge movement from around Ti atoms to around Cl, O, and S.

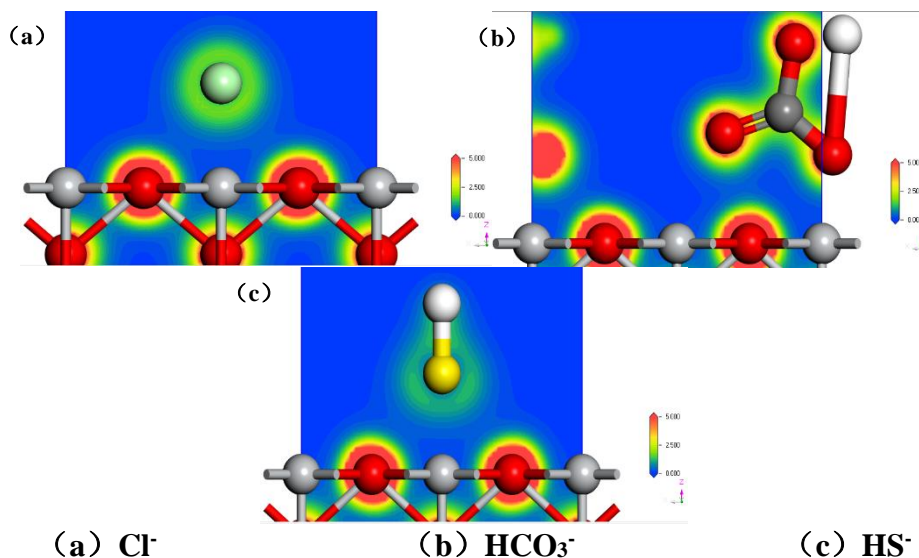


Figure 9. Charge density distribution at the interface between different corrosive ions and TiO_2

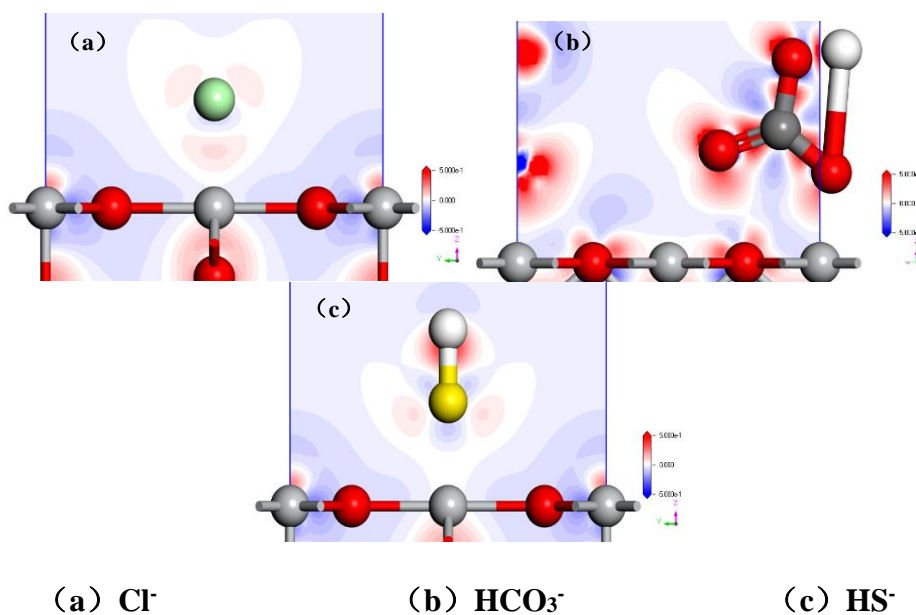


Figure 10. Differential charge density distribution at the interface between different corrosive ions and TiO_2

In order to further investigate the nature of electronic interactions for interfacial bonding after adsorption occurs, the steady-state adsorption configurations of the above three anions on the $\text{TiO}_2(1\ 1\ 0)$ surface were analyzed by the density of partial wave states (PDOS), and the PDOS curves of single Cl^- ion, single HCO_3^- ion, and single HS^- ion adsorbed on the $\text{TiO}_2(1\ 1\ 0)$ surface are shown in Figs. 11(a)~(c), respectively.

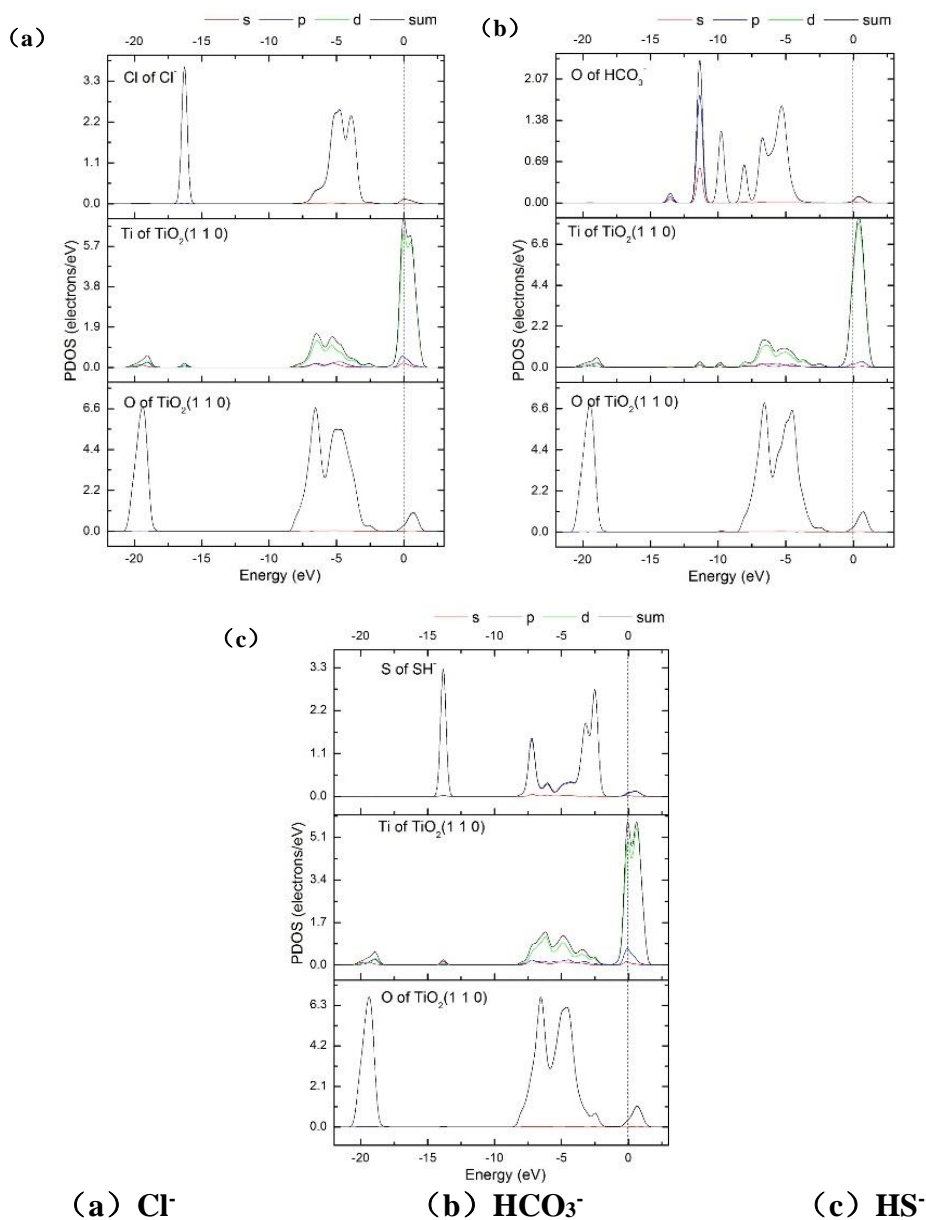


Figure 11. PDOS curves of different corrosive ions after adsorption on Ti(110) surface

The charge interactions between the Cl atom in the Cl⁻ ion, the O atom in the HCO₃⁻ ion, and the S atom in the HS⁻ ion and the Ti atom on the TiO₂ surface respectively occur in the -17eV and -5eV, -3eV to -7.5eV, and -2eV to -3.5eV energy level intervals, and are mainly caused by the 3d2 electrons of the Ti atom and the 3p5 of Cl, 2p4 of O, and S 3p4 electrons between the hybridization orbitals of the Ti atom[35].

3.3.2 Interfacial binding energy between different aggressive ions and TiO₂ (110) surfaces

The TiO₂ interfacial model after geometrical optimization is visualized in Fig. 12. It can be seen that the model after chirality shows a disordered atomic structure in a very narrow region near the interface, which can be regarded as an interfacial transition or reaction layer[34]. Table 5 shows the

interfacial binding energy of a neutral environment and corrosive gases H₂S and CO₂ with TiO₂ at different temperatures with different Cl⁻ concentrations. According to the more negative value of the end state minus the beginning state means that the end state is more stable, the easier it is to change from the beginning state to the end state, the thermodynamic stability of TiO₂ gradually decreases as the temperature increases at a certain Cl⁻ concentration. When the Cl⁻ concentration increases, the binding energy value decreases, the easier the corrosive ions are combined with the TiO₂ surface, then stronger its aggressiveness. It implied that as the temperature or the concentration of Cl⁻ increases, its aggressiveness to the TiO₂ surface becomes stronger, and the thermodynamic stability of TiO₂ passivation film is weakened. Once the concentration of Cl⁻ and temperature are fixed, the addition of H₂S and CO₂ will make it easier for Cl⁻ to bind with the rutile TiO₂ (110) surface, i.e. the potential barrier needs to be surpassed for the adsorption of Cl⁻ on the (110) crystal surface is smaller, and the thermodynamic stability of TiO₂ passivation film is also less thermodynamically stable.

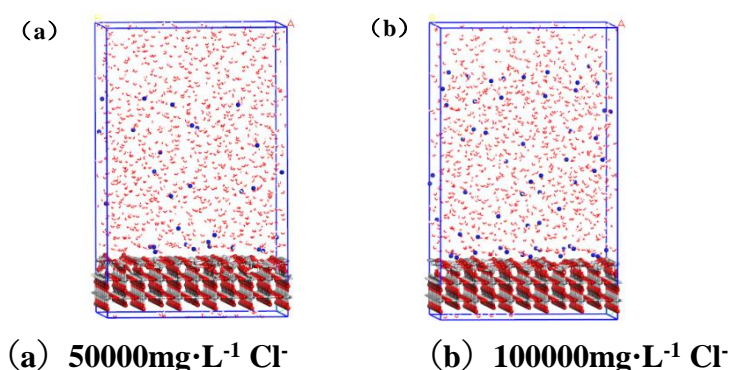


Figure 12. Geometrically optimized TiO₂ interface model

Table 5. Interfacial binding energy with TiO₂ under different corrosion conditions

Cl ⁻ concentration (mg·L ⁻¹)	Temperature (°C)	Combined energy (Kcal/mol·Å ⁻²)		
		Neutral environment	CO ₂ environment (p _{CO2} =5MPa)	H ₂ S environment (p _{H2S} =5MPa)
50000	180	-22.0961	-22.3119	-22.3483
	230	-22.5116	-22.5639	-23.7228
100000	180	-24.2596	-24.2268	-24.4753
	230	-24.5288	-24.75772	-24.8472

4. CONCLUSIONS

(1) The uniform corrosion of TC4 titanium alloy in the neutral environment, CO₂-containing and H₂S environment is relatively mild, and no obvious pitting corrosion occurs. The uniform corrosion rates

in the three environments are $0.0004 \text{ mm}\cdot\text{a}^{-1}$, $0.0004 \text{ mm}\cdot\text{a}^{-1}$ and $0.0009 \text{ mm}\cdot\text{a}^{-1}$, indicating that it has good resistance to uniform corrosion and local corrosion.

(2) The anodic polarization curves of TC4 titanium alloy in neutral environment, CO_2 -containing and H_2S -containing environments have obvious passivation zones, the corrosion reaction is controlled by anodic process. And the passivation films are all n-type semiconductors, which can repel the erosion of the metal substrate such as Cl^- . At a certain temperature, the self-corrosion potential of TC4 titanium alloy decreases and the corrosion driving force increases after the addition of CO_2 and H_2S compared with the neutral environment. As the breakdown potential and protection potential of the passivation film reduced, the polarization resistance is significantly decreased, and the electrochemical corrosion kinetic hindrance performance is weakened. the increase of donor concentration for the passivation film results in the deterioration of its corrosion resistance. In particular, TC4 titanium alloy is most susceptible to corrosion in the H_2S environment.

(3) Three corrosive ions Cl^- , HCO_3^{3-} and HS^- have strong charge interactions with Ti atoms on the TiO_2 (110) surface. Interfacial bonding mainly exists between Cl, O, S of Cl^- , HCO_3^{3-} and HS^- three ions and Ti atoms, and the bonding is mainly due to charge movement from around Ti atoms to around Cl, O, and S. Charge bias around the negatively charged ions while charge dissipation around the surface Ti atoms. The interfacial bonding is mainly due to the electron orbital hybridization produced by $\text{Cl}-3p_5$, $\text{O}-2p_4$, $\text{S}-3p_4$, and $\text{Ti}-3d_2$. When the Cl^- concentration and temperature are fixed, the addition of H_2S and CO_2 will make the Cl^- bond with the rutile TiO_2 (110) surface more easily, and the thermodynamic stability of the TiO_2 passivation film became worse.

ACKNOWLEDGEMENT STATEMENT

This work is supported by the National Natural Science Foundation of China (NSFC) (Contract Nos. 51902254 and 51701157) and the Natural Science Foundation of Shaanxi Province (Nos. 2018JM5108 and 2022JM-261).

References

1. F. Argall, *Solid-State Electron.*, 11 (1968) 535-541.
2. F.F. Zhang, C. Feng, L. J. Zhu and W.W. Song, *Mater. Sci. Forum*, 1035 (2021) 528-533.
3. Y.W. Fu, L. Zhao, Y. Zhao, H. Zhao, J. Cui and M. Chen, *Oil Drilling and Production Technology*, 39 (2017) 662-666.
4. X.X. Lv, Y. Shu, G.X. Zhao, J.F. Xie and Y. Xue, *Rare Met. Mater.Eng.* 43 (2014) 1518-1524.
5. C.C. Liu, G.M. Ke and Y. Li, *Nat. Gas Ind.*, 39 (2019) 149-155.
6. R.D. Kane, B. Craig and A. Venkatesh, *64th NACE Annual Conference*, (2009), Houston: Omnipress.
7. B. Hargrave, M. Gonzalez, K. Maskos, J. Skogsberg, and J. Grauman, *65th NACE Annual Conference*, (2010), Houston: Omnipress.
8. J. Liu, A. Alfantazi and E. Asselin, *71th NACE Annual Conference*, (2016), Houston: Omnipress.
9. M.O. Bodunrin, L.H. Chown, J.W.V.D. Merwe, K.K. Alaneme and N.P. Mphasha, *Corros. Rev.*, 38 (2020) 25-48.
10. X.Y. Wang, S.D. Zhu, Q. Liu, A.Q. Fu and J.L. Li, *Mater. Sci. Forum*, 1032 (2021) 195-200.
11. S.F. Zhao, H.G. Jia and J.H. Wang, *Applied Mechanics and Materials*, 599 (2014) 169-178.
12. G.Z. Deng, *Titanium Metallurgy*, (2010), Beijing: Metallurgical Industry Press.

13. B. Pazhanivel, P. Sathiya, K. Muthuraman and G. Sozhan, *Eng. Fail. Anal*, 127 (2021) 105515.
14. J.P. Perdew, Y. Wang, *Phys. Rev. B: Condens. Matter*, 145 (1992) 13244-13249.
15. Y.Q. Pan and L.X. Hang, *Chinese Journal of Lasers*, 38 (2011) 180-184.
16. X. Xing, W.J. Wang, S.H. LI, Y.L. Liu, D. Zhang and Q. Shi, *Chinese Journal of Lasers*, 40 (2013) 0207001.
17. R.W. Schutz. *Corrosion*, 244 (1995) 1-20.
18. F. Hua, K. Mon, P. Pasupathi, G. Gordon, D. Shoesmith, *Corrosion*, 10(2005):61.
19. J. Li , F. Wu, J. Shi, L. Ma and S. Zheng, *Mater. Sci.-Pol.*, 38 (2020) 253-262.
20. Z.Z. Duan, Q. Wei, *Acta Geol. Sin.*, 85 (2011)1079-1093.
21. M.J. Chen, D.P. SONG, Y.C. Liang China International Nanotechnology Symposium, (2007).
22. NACE SP 0755-2013S.. 2013
23. W.P. Gao, X.X. Lv, J. F. Xie, J. Ling, M. F. Zhao, J. J. Liang, W. Liang and G.X. Zhao, *Rare Met. Mater.Eng.*, 47 (2018) 151-156.
24. J.D. Li, C. Chen, S.G. Zhang, B. Lin, Y.Y. Wang, Y.Q. Zhu and Y.L. Tang, *Surf. Technol.* 50 (2021) 101-115.
25. X.X. Lv, L.L. Liu, L. Jian, H. B. Yu and J. F. Xie, *Rare Met. Mater.Eng.*, 49 (2020) 2326-2332.
26. X.J. Yang, C.W. Du, H.X. Wan, Z. Y. Liu and X. G. Li, *Appl. Surf. Sci.*, 458 (2018) 198-209.
27. N. Momin, J. Manjanna, S.T.Aruna , S. Senthilkumar, D.S. Reddy, A. Kumar, *J. Chem. Sci.*, 134 (2022) 1-11.
28. V. Bessergenev, *Mater. Res. Bull.*, 44 (2009) 1722-1728.
29. N.F. Mott, *Phys. Sci.* 171 (1939) 27-38.
30. D.D. Macdonald, *J. Electrochem. Soc.* 137 (1990) 2395.
31. P. Wu, X. Zhu, L. Xu, W. Peng and G. Zhao. *Electrochem. Commun.* 118 (2020) 106793.
32. Y. Tan, N.N. Aung, T. Liu, *Corros. Sci.*, 63 (2012) 379-386.
33. X.Y. Wang, S.D. Zhu, Z. G. Yang, C. D. Wang, N. Wang, Y.Q. Zhang and F.L. Yu, *Mater.*, 15 (2022) 4381.
34. Q. Feng, X.Q. Wang and G.B. Liu, *Journal of Atomic and Molecular Physics*, 73 (2008) 3202.
35. Y.Y. Li., *Journal of Xi'an Shiyou University(Natural Science Edition)*, 33 (2018) 120-126.